Charge injection into organic semiconductors

Woudenbergh, Teunis van

Chapter 5

Charge injection across a polymeric heterojunction

5.1 Introduction

A typical polymeric light-emitting diode (PLED) consists of a thin layer of undoped conjugated polymer sandwiched between two electrodes. Experimentally, attention has especially been focused on PLEDs that contain the conjugated polymer poly(phenylene vinylene) (PPV) or its derivatives which have an external conversion efficiency larger than 1% photons/charge carrier [14]. The electron conduction in the PPV-derivatives proved smaller than the hole conduction, which was attributed to the presence of traps [13] or lower electron mobility [30]. For PLEDs, in which both electrons and holes are injected, the different conduction of electrons and holes is directly responsible for the distribution of the light-output in the polymer layer. Model calculations of a PLED with Ohmic contacts showed that the light-output is mainly confined in a region close to the cathode, due to the reduced electron conduction [13]. As a result non-radiative energy transfer to the metallic cathode strongly reduces the quantum efficiency (photon/charge carrier) of the PLED at low voltages. The use of heterojunctions has proven to be very useful, as has been demonstrated in LEDs based on evaporated small molecules (OLEDs). In these multilayer OLEDs the active part consists of various layers with various functions, leading to highly efficient devices [80]. These layers are chosen to have properties such as hole and electron transport, hole or electron blockage and high emission. For PLEDs the preparation of multilayers from solution is more problematic because the bottom layer can be dissolved during application of a subsequent layer. The opto-electronic properties of organic multilayer devices are strongly dependent on the offset in band-edge positions. For example, the presence of a large energy barrier at an interface blocks high mobile charge carriers and prevents radiative losses near the metal electrodes. This feature will be employed in detail in this chapter: in the first part of this chapter, the functional dependence on electric field and temperature of the hole injection across a heterojunction will be investigated. In the last part, the consequences of a hole blocking layer for the performance of a heterojunction PLED will be studied.

Recently, a theoretical model describing charge transport across an interface from one or-

ganic dielectric into another has been developed by Arkhipov et al. [81]. So far, no systematic experimental study has been conducted to investigate the charge transport across organic-organic interfaces. Attention has mainly been focused on the injection of charges from a metallic electrode into an organic dielectric. For inorganic semiconductors the charge injection is described by thermionic emission and tunneling [23]. For organic semiconductors on the other hand the charge injection is governed by hopping of charge carriers into localized sites that are energetically disordered [53]. This energetic disorder is caused by fluctuations in the energy of the localized transport sites, described by a Gaussian DOS with a width σ of typically 0.1 eV [12]. The presence of energetic disorder is expected to strongly reduce the T-dependence of the charge injection process, as has been experimentally confirmed by studies on PPV (chapter 2,Ref. [64]). A fundamental difference between charge transport across an organic-organic interface (OOI) and a metal-organic interface (MOI) is that for an MOI the image charge potential causes a barrier lowering, which strongly influences the field dependence of the charge injection [53]. For an OOI, low carrier concentrations and slow dielectric relaxation in the "electrode"(injecting layer) do not allow the creation of an image charge, and the image potential is absent. Therefore, it is expected that the charge transport across an OOI is only weakly field dependent as compared to the MOI [81].

In the present study the charge injection across a polymeric heterojunction is investigated. The heterojunction is formed by a poly-p-phenylene vinylene (PPV) hole injecting layer with a poly(9,9-dioctylfluorene) (PFO) hole accepting layer on top. For such a system, an interface energy barrier for hole transport is formed between the PPV and the PFO due to the offset between the highest occupied molecular orbitals (HOMOs) of both polymers (inset figure 5.3). PPV has a HOMO of 5.3 eV [16], while for PFO the HOMO is about 5.8 eV [17], resulting in an interface energy barrier of $\phi_b \sim 0.5$ eV. It is demonstrated that such a large injection barrier strongly limits the hole current across the heterojunction. At high applied voltages the weak field dependence of the current across the polymeric heterojunction is in agreement with the predictions of the model from Arkhipov et al. [81]. At low fields the experimental current shows a stronger field dependence as compared to the model. This is attributed to a change of the effective barrier height due to the filling of states at the injecting interface.

5.2 Injection model for organic-organic interfaces

The description of the injection current in the OOI model resembles much of the injection model for a metal organic interface. Here too, the injection process is a two-step process: an initial upward jump that determines most of the field and T-dependence, followed by a diffusive escape, as is also shown in figure 5.1. The analytical description is given by

$$J \propto \int_a^\infty dx_0 \exp(-2\gamma\, x_0) \int_{-\infty}^\infty dE \mathrm{Bol}(\phi_b + E - x_0 F_{PFO}) g(E) w_{esc}(E, x_0). \qquad (5.1)$$

In the analytical model, it is assumed that a carrier starts from a fixed energy level in the injecting layer, and jumps to an arbitrary energy level in the accepting layer, governed by the Boltzmann statistics (equation 1.26). It can also be injected to an arbitrary distance from the interface, x_0, except for distances smaller than the nearest neigbour distance a, as it is assumed that no transport sites are present for $x_0 < a$. The jump rate to a certain distance x_0 is given by the

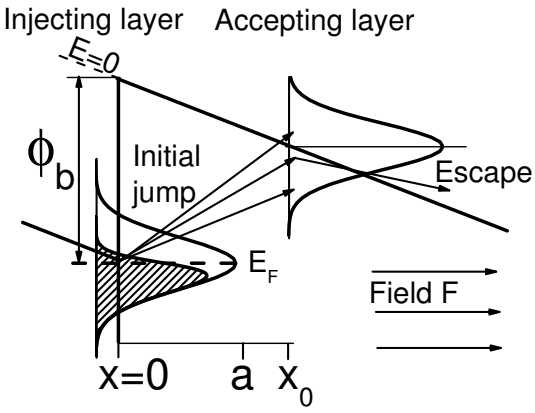

Figure 5.1: Schematic representation of the injection across a polymer heterojunction. The barrier height amounts to ϕ_b, due to an electric field F, the band in both materials will tilt. The injection process consist of an initial jump to a target site at $x = x_0$, followed by an escape probability deeper into the polymer. The carrier has to jump to a target site with $x_0 \geq a$, the nearest neighbour distance. For reasons of calculation, zero energy $E = 0$ is taken along the tilted band in the accepting layer. It is assumed that all jumps take place from the Fermi-level in the injecting layer, which is at $E_F = E = -\phi_b$ for a half-filled DOS.

fall-off of the electron wave-function on the start-site, $\exp(-2\gamma x_0)$. This is similar to the case of an MOI, described in paragraph 1.4.

The difference is the absence of the image force lowering term, which has consequences both for the energy level to which the charge carriers are injected, $\phi_b + E - x_0 F_{PFO}$, and for the form of the escape probability w_{esc}. A carrier that has been injected across the heterojunction resides on the target side at place x_0 and with energy E. It can either jump back into the injecting layer, or jump forward, further into the accepting layer. If the jump across the interface was upward, the jump back will be given by $\nu_{back} = \nu_0 \exp(-2\gamma\ x_0)$. The escape probability w_{esc} can then be found as follows: First find the average number of neighbours $n_i(x_0, E)$ in a hemisphere around the target side in forward direction. Then, the Poisson distribution tells that the chance to actually find such a neighbour is $w_{esc} = 1 - \exp\left[-n_i(x_0, E)\right]$.

To calculate the average number of neighbour sites, one should in principle perform the calculation for a complete device. But due to the rapid fall-off of the tunneling factor $\exp(-2\gamma\ x)$ only sites with a transition rate $\nu_{forward} \leqslant \nu_{back}$ have to be taken into account. For downward forward hops over a distance r, $\nu_{forward} = \nu_0 \exp(-2\gamma\ r)$ and this means that $r \leqslant x$. For upward forward hops, with an energy difference $E' - E$, $\nu_{forward} = \nu_0 \exp(-2\gamma\, r) \exp(-\frac{E'-E}{kT})$. With the requirement of a larger forward hop rate than the jump-back rate, the cut-off is given by $(E' - E)/kT + 2\gamma r \leqslant 2\gamma x$, so that the energy E' of the neighbour site to which the carrier wants to hop obeys to $E' \leqslant E + 2\gamma kT(x - r)$. Due to the applied field F the band tilts. As E and E' are defined with respect to the center of the Gaussian $g(E)$ (see figure 5.1, the cut-off becomes $E' \leqslant E + 2\gamma kT(x - r) + Frz$. In this equation, $z = cos(\theta)$, with θ being the angle

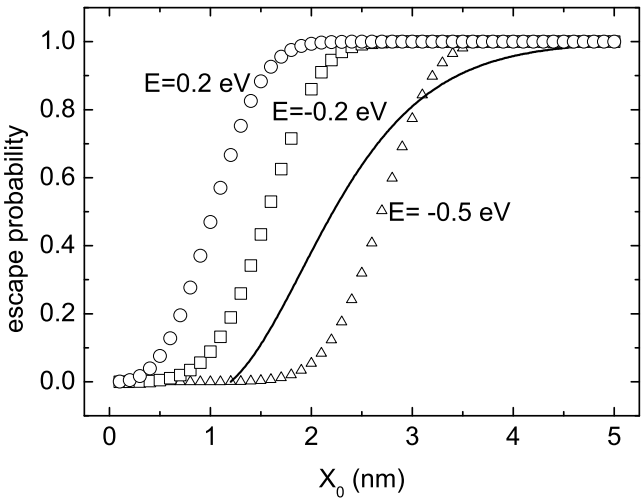

Figure 5.2: Calculated escape probabilities for the OOI model for three different energies as indicated in the figure. The Onsager Escape probability, equation 1.27), is plotted as a solid line.

between field and jump direction. The number of neighbours that give rise to forward jumps is then given by

$$n_i = 2\pi \int_0^{x_0} dr r^2 \int_0^1 dz \int_{-\infty}^{E+2\gamma kT(x_0-r)+eFrz} dE' g(E'). \tag{5.2}$$

In figure 5.2 the escape probabilities $w_{esc}(x_0, E)$ as a function of target site distance x_0 from the heterojunction-interface are compared for a number of energies. For target sites deeper in the Gaussian distribution (e.g. $E = -0.5$ eV), the escape chance is smaller than charges that jump onto target sites with high energies (e.g. $E = 0.2$ eV). For the latter, more neighbours are accessible and as a result the escape from the heterojunction interface is more probable. To illustrate the impact of the image force on injected carriers, the Onsager escape probability (equation 1.27) is also plotted in figure 5.2, using the same parameters. For clarity, the Onsager escape probability is not applicable to OOIs. It is observed that the escape probability at the OOI, for injection energies around the center of the Gaussian ($E = 0.2$ eV and $E = -0.2$ eV), is larger than the Onsager escape. This is due to the absence of image force in the OOI: charge carriers that surpass the barrier experience a field in forward direction and have a large chance to escape. For the MOI, the carriers experience a field towards the contact before they pass the potential maximum (see figure 1.10) due to image force.

5.3 Experiment

In this study we have made double layer structures with a bottom layer of a PPV derivative, spincoated on top of ITO, followed by a spincoated top layer of PFO. The bottom PPV-based

layer is a random copolymer of poly[2,5-bis(2'-ethylhexyloxy)-1,4-phenylenevinylene] (BEH-PPV) and poly[2,5-bis(2'-methylbutyloxy)-1,4-phenylenevinylene] (BMB-PPV). By changing the ratio between the highly soluble BEH-PPV and the insoluble BMB-PPV the solubility of the copolymer can be tuned, without changing its charge transport properties [82]. In a 1:3 BEH-co-BMB-PPV ratio the film can be spin casted from chloroform and is insoluble in toluene, which permits spincasting of the PFO layer on top. Via thickness measurements it has been confirmed that the thickness of the two-layer devices equals the thickness of two separate layers (PPV and PFO), prepared with the same spin-coat conditions. Two batches have been used. For one the bottom layer is $d_{PPV} = 100$ nm, with a top layer of $d_{PFO} = 70$ nm, the other batch has a bottom layer $d_{PPV} = 140$ nm ($d_{PFO} = 100, 140, 230$ nm). On top of the PFO a Au contact has been evaporated. For such a device (inset figure 5.3), the bottom ITO electrode forms an Ohmic contact on PPV, while the Au top contact blocks electron injection into the PFO layer, and the current throughout the device is carried by holes (hole only device). As a reference, single layer hole only devices have been made, where the ITO bottom electrode has been covered with the BEH-PPV derivative, and on top a Au electrode has been evaporated.

5.4 Results

5.4.1 Injection-limited transport across the polymeric heterojunction

In figure 5.3 the current-density voltage ($J - V$) characteristic of a PPV/PFO double layer device is shown. The thicknesses amount to $d_{PPV} = 140$ nm and $d_{PFO} = 230$ nm for the PPV and PFO, respectively. It is observed that the current of the two layer PPV/PFO devices is indeed strongly reduced with respect to the PPV single layer device. The dashed line is the SCL hole current calculated with a field-dependent mobility as given by equation 1.14. A zero-field mobility $\mu_0 = 1.5 \times 10^{-10}$ m^2/Vs and a field activation factor $\alpha = 3 \times 10^{-4}$ m^2/Vs have been obtained. As a reference also the maximum attainable current for the double layer device is calculated: This current is reached when the OOI energy barrier is not present and the current is only limited by the build-up of space charge in the two layers. The solid line shows the calculated device current for such a SCLC two layer device. For the mobility of PFO, $\mu_0 = 1 \times 10^{-9}$ m^2/Vs and $\alpha = 5 \times 10^{-5}$ m^2/Vs have been used (chapter 4 and [83]). It is observed that at low voltages the measured current density for the two-layer device (triangles) is more than three orders of magnitude lower than the calculated bulk SCLC (solid line), which indicates that the current across the heterojunction is indeed strongly injection-limited. From this observation it is expected that the field-distribution across the PFO layer is uniform, since the amount of charge carriers entering the PFO is too small to locally change the field. It should be noted that this constant electric field in the accepting PFO layer, F_{PFO}, determines the charge transport across the heterojunction interface, as can be seen from equation 5.1 [81].

In order to verify this scaling the current-density through the two-layer device has been plotted as a function of V/L_{PFO} in figure 5.4a, for different thicknesses of the PFO top layer. For low electric field ($F_{PFO} < 8 \times 10^7$ V/m), the V/L_{PFO} scaling is indeed approached. However, at higher fields the current for thinner PFO top layers is substantially reduced, indicating that apparently not all voltage drops across the PFO layer. For very thin top PFO layers an eventual voltage drop across the bottom PPV injecting layer can have a relatively large influence on the

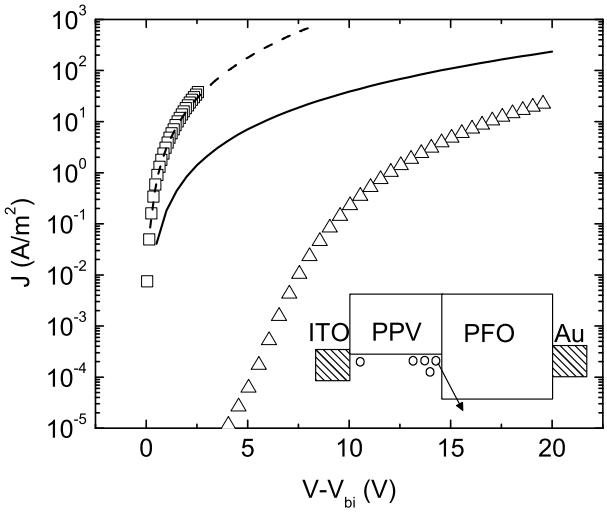

Figure 5.3: Current density as a function of voltage for an ITO/PPV/Au hole-only device ($d = 140$ nm) (squares) together with an ITO/PPV/PFO/Au double layer device ($d = 140 + 230$ nm) (triangles). The dashed line is the calculated space charge limited current (SCLC) through the single layer device, the solid line depicts the calculated SCLC through the double layer, using the bulk transport parameters of each layer, in the absence of an interface barrier. The inset shows the schematic energy band diagram of the double layer device.

electrical characteristics. It is important to realize that the charge transport through the PPV-based injecting layer is space-charge limited. As a result this layer only becomes conductive when charge is injected into it. Since this charge is not neutralized it will lead to a built-up of electric field in the PPV, and subsequently to a substantial voltage drop across this layer. In order to analyze the field-dependence of the injection-limited current across the OOI, knowledge about the field F_{PFO} is indispensable. Therefore, the applied voltage needs to be corrected for the voltage drop across the bottom PPV layer.

5.4.2 Potential drop across the PPV injecting layer

For SCL transport the current is proportional to the total amount of injected charges, which makes it possible to decouple the hole transport in the PPV and the transport across the heterojunction. In case of a field-independent mobility the voltage drop across the PPV (V_{PPV}) for a given current-density J of the double layer device is simply given by (ε the dielectric permittivity)

$$V_{PPV}^2 = \frac{J d_{PPV}^3}{\frac{9}{8}\varepsilon\mu}. \tag{5.3}$$

As an example, for a current density of $J = 10$ A/m^2, a thickness of $d_{PPV} = 140$ nm for the PPV bottom layer, and a mobility of $\mu_0 = 1.5 \times 10^{-10}$ m^2/Vs, the voltage drop over the PPV

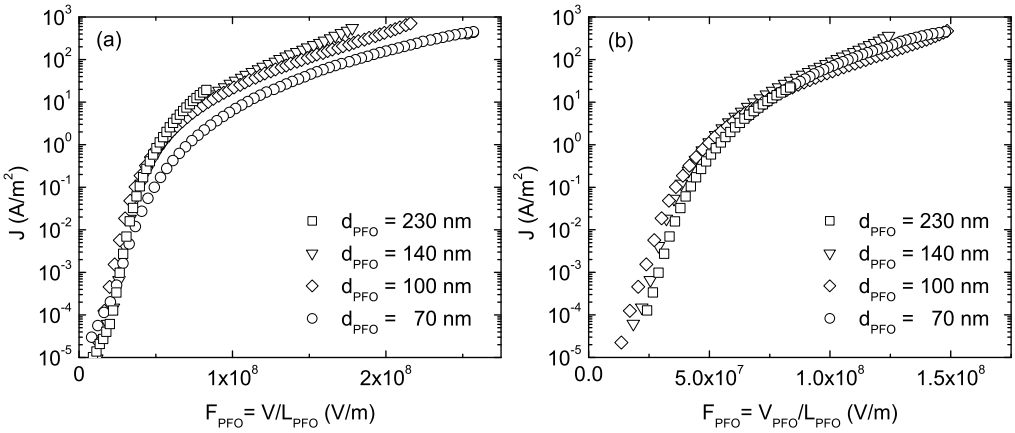

Figure 5.4: Current density J versus the electric field F_{PFO} in the accepting layer, (a) with the voltage drop across the accepting layer equal to the applied voltage, $F_{PFO} = V/L_{PFO}$, (b) with the applied voltage being corrected for the voltage drop across the PPV bottom layer, $F_{PFO} = (V - V_{PPV})/L_{PFO}$. One double layer device consists of a PPV bottom layer with $d_{PPV} = 100$ nm and a top PFO layer of $d_{PFO} = 70$ nm, the other devices have a PPV bottom layer of $d_{PPV} = 140$ nm and top PFO layers of $d_{PFO} = 100, 140$ and 230 nm, respectively.

layer is about 2.5 V, while the experimental voltage drop over the total device is about 9 V for a PFO thickness of $d_{PFO} = 100$ nm to 18 V for $d_{PFO} = 230$ nm. As a result for a thin PFO top layer (100 nm) this 2.5 V amounts to almost one third of the total voltage drop. In case of a field-dependent mobility the voltage drop can be solved numerically from the one-carrier SCLC model [19]. It should be noted that such a procedure correctly provides the voltage drop across the PPV-layer of the heterojunction device, since both current and voltage drop are related to the total amount of charge inside the layer. However, the field- and carrier density distribution of the single carrier SCLC model are not applicable to the heterojunction device; in the heterojunction device there will be a large built-up of charge carriers at the blocking junction, as will be later discussed in the device model for the double layer device.

With V_{PPV} known, the voltage drop and field across the PFO layer follows directly from

$$V_{PFO} = V - V_{PPV}. \tag{5.4}$$

The electric field F_{PFO} in the PFO top layer now becomes $F_{PFO} = V_{PFO}/d_{PFO}$. Figure 5.4b shows the resulting $J - F_{PFO}$ plots for the various double layer devices. It is observed that J scales with F_{PFO}, as expected for an injection-limited device. Thus figure 5.4b represents the $J - F_{PFO}$ relation of the experimental injection-limited current across the PPV-PFO heterojunction.

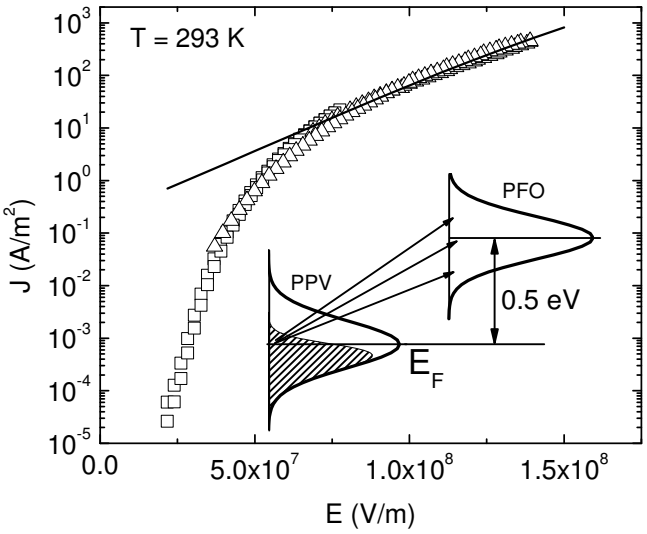

Figure 5.5: $J - F_{PFO}$ characteristic for $d_{PFO} = 230$ nm (squares) and $d_{PFO} = 70$ nm (triangles) device at room temperature, together with the calculated injection current from the OOI model (solid line). The inset shows the half filled DOS of the PPV at the heterojunction interface, the charge carriers jump from the center of the Gaussian into the states of the PFO, as assumed in the OOI model [81].

5.4.3 Comparison of the experiment with the OOI model

As next step the injection current from PPV into PFO has been compared with the injection model for organic hetero-interfaces (OOI model) [81]. As an input for this model, the energy distribution width and the nearest neighbour distance in the accepting layer should be known. The width of the distribution, σ, has been taken from TOF measurements on PFO, $\sigma = 0.1$ eV [84]. The nearest neighbour distance can be estimated from the length of a PFO monomer, $a_{PFO} \sim 1$ nm. Furthermore, the barrier height amounts to ~ 0.5 eV. An inverse localization radius $\gamma = 5 \times 10^9$ m^{-1} has been used [56]. As shown in the inset of figure 5.5 in the theoretical model it is assumed that the DOS at the PPV interface is filled up to the center of the Gaussian distribution, and the charge carriers therefore jump from the maximum of the Gaussian DOS [81]. Using these parameters, the injection current across the OOI can directly be calculated. In figure 5.5, the injection current calculated from the OOI model is plotted together with the experimental characteristics for $T = 293$ K. At higher electric fields ($F_{PFO} \gtrsim 7 \times 10^7$ V/m) the experiment is well described by the OOI model. The calculated injection current from the OOI model in this field range is only weakly field dependent.

For comparison, in figure 5.6 the current across the polymeric heterojunction is plotted together with the ILC from a Pt bottom electrode into the PFO layer. For the freshly evaporated Pt we measured a work function of ~ 5.0 eV in nitrogen atmosphere. This leads to a hole injection barrier of about $\sim 0.8 - 0.9$ eV, also resulting in a strongly injection-limited current.

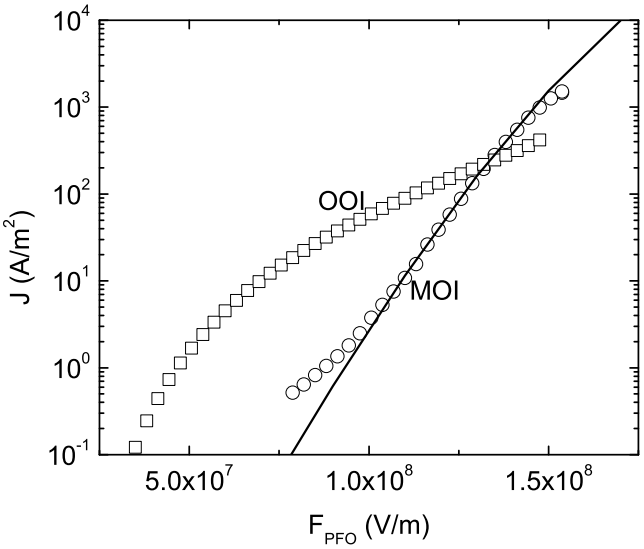

Figure 5.6: The injection-limited current across a PPV/PFO interface (OOI, squares) together with the injection current from a Pt anode into PFO (circles). The measurement of the heterojunction is corrected for the voltage drop across the PPV layer. The solid line is a calculation of the injection current for a MOI with $\phi_b = 0.9$ eV.

The ILC from the metallic electrode is modeled with the hopping based injection model [53]. As expected, the absence of image force lowering in the organic-organic heterojunction leads to a strong reduction of the field dependence as compared to the injection from a metallic electrode [81].

At low fields there is a large discrepancy between the experimental current and the OOI model. In the model it is assumed that the starting energy for a carrier jump across the OOI is the middle of the Gaussian DOS of the injection layer. However, for an organic heterojunction between two disordered materials this starting energy is not a well defined value, as will be discussed in the next paragraph.

5.5 Discussion

5.5.1 Influence of carrier concentration

For injection of charges from a metal contact into an organic dielectric the starting point for a charge carrier jump is always the metal Fermi-level, independent on the injection current density. However, for an organic heterojunction, the Fermi-level from where a charge carrier is injected does depend on the injection current, because the charge carrier concentration at the interface changes with current, as indicated in the inset of figure 5.10. In a disordered semiconductor the charge carrier mean energy is at σ^2/kT below the center of the Gaussian DOS for low carrier

concentrations [12], as shown in figure 1.7. This mean energy is then the starting point for injection of charges across the heterojunction. However, with increasing carrier concentration the Fermi-level passes the equilibrium energy, $E_F > -\sigma^2/kT$, and the energy level from which the charge carriers are injected now rises with E_F. Assuming thermal equilibrium, the Fermi level is found from:

$$p = \frac{N_{sites}}{\sqrt{2\pi}\sigma} \int_{-\infty}^{\infty} \mathrm{dE} \frac{\exp\left(-\frac{1}{2}\left(\frac{E}{\sigma}\right)^2\right)}{1+\exp\left(\frac{E-E_F}{kT}\right)}, \tag{5.5}$$

where N_{sites} is the concentration of localized sites in the PPV. In the original OOI model [81], two situations have been described; One for a half-filled DOS (figure 5.1) where the injection energy level equals the center of the Gaussian distribution ($E_{inj} = 0$), and one for very low carrier densities, where the injection energy level equals the equilibrium energy, $E_{inj} = -\sigma^2/kT$. However, the OOI model can be applied to an arbitrary injection energy, which results in an effective barrier height, $\phi_{b,eff} = \phi_b - E_{inj}$. As described above the additional injection energy E_{inj} is given by

$$E_{inj} = \begin{cases} E_F, & E_F > -\dfrac{\sigma^2}{kT}, \\ -\dfrac{\sigma^2}{kT}, & E_F < -\dfrac{\sigma^2}{kT}, \end{cases} \tag{5.6}$$

where E_F is found from equation 5.5.

5.5.2 Drift-diffusion device model

In order to take the filling of interface states into account, the charge carrier density at the heterojunction has to be calculated as a function of applied field or voltage. For this we use a numerical drift-diffusion device model developed in our group [85]. The device model has been used as follows: For the PPV bottom layer, the hole transport parameters are known, and as a result the concentration throughout this layer can be calculated for a certain current density. This charge distribution is fixed by the boundary charge densities: At the ITO anode, all the states are filled (Ohmic contact), whereas at the heterojunction the charge density is unknown, and so the interface concentration p_{int} is guessed. Concurrent with the charge distribution also the field distribution and resulting voltage drop are calculated. As a result, for a certain guess of p_{int}, the electric field at the heterojunction interface $F_{PPV,int}$ as well as the voltage drop across the PPV layer V_{PPV} are also obtained.

As input for the device model, the measured current density J, together with the applied bias V (corrected for a small built-in voltage) are used. As the device model calculates the voltage drop across the PPV layer, V_{PPV}, also the voltage drop across the PFO layer $V_{PFO} = V - V_{PPV}$ and thus the electric field $F_{PFO} = V_{PFO}/L_{PFO}$ are known. Then we make use of a property of an electric field at an interface: the electric field $F_{PPV,int}$ at one side of the interface is connected to the electric field across the PFO layer F_{PFO} at the other side of the interface via $F_{PPV,int} = \frac{\varepsilon_{PFO}}{\varepsilon_{PPV}} F_{PFO}$. Due to the small difference in dielectric permittivity for polymers ($\varepsilon_r \sim 3$), this condition reduces to $F_{PPV,int} = F_{PFO}$. Running the device model will return a field $F_{PPV,int}$, together with a field F_{PFO} depending on the charge distribution. Therefore, we can make a loop, where the concentration p_{int} of holes in the PPV at the heterojunction

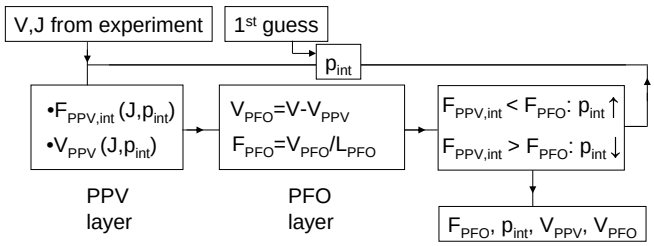

Figure 5.7: Flow-chart of the operationalization of the drift-diffusion device model: as input the experimentally measured current density J and bias V are used. Then with a given J and choosing an interface concentration p_{int}, the voltage drop V_{PPV} and interface field $F_{PPV,int}$ are calculated. With V_{PPV}, the voltage drop and the electric field across the PFO layer are calculated (second block). Comparing $F_{PPV,int}$ with F_{PFO} results in a decision for the new value of p_{int} as is described in the text, see also 3rd block. The calculation is looped until a desired precision in the comparison of $F_{PPV,int}$ and F_{PFO} is reached. This results in the value of p_{int}. As a by-product, also the voltages across the PPV layer and PFO layer are returned.

interface is the variable, and $F_{PPV,int} = F_{PFO}$ is the condition. As long as the condition is not obeyed, the concentration p_{int} has to be adapted. For a large p_{int}, the charge concentration close to the heterojunction interface is enhanced, resulting in a higher $F_{PPV,int}$. Similarly, a smaller p_{int} results in a lower value of $F_{PPV,int}$. At the same moment, the field F_{PFO} is rather insensitive to the chance of the interface concentration. As a result, the value of p_{int} must be adapted according to the following scheme

$$p_{int} : \begin{cases} \text{if } F_{PPV,int} < F_{PFO} : & \text{increase } p_{int}, \\ \text{if } F_{PPV,int} > F_{PFO} : & \text{decrease } p_{int}, \end{cases} \tag{5.7}$$

and the device model is re-runned. For each run the whole charge concentration throughout the PPV layer is recalculated. When the difference between $F_{PPV,int}$ and F_{PFO} is small enough the device model stops and p_{int} is returned. This scheme is also given in figure 5.7.

From the drift-diffusion model also the voltage drop across the PPV layer is obtained. For the different iterations of the device model, when it adapts the interface concentration p_{int}, it is already observed that the voltage drop V_{PPV} is nearly constant, which means it is insensitive to the actual charge distribution in the device. This is also demonstrated in figure 5.8, where as a function of device current the measured voltage drop across the single-layer PPV device is shown, together with the voltage drop across the PPV in i) the single layer device, calculated with an equation based on drift current, and ii) the double layer device, calculated with the drift-diffusion model. There is only a small deviation between the measured single layer and calculated double layer voltage drop V_{PPV}, indicating the insensitivity of the voltage to the actual charge distribution. As a direct result, the decoupling of the two layers to find the voltage drop for each layer is justified (equations 5.3,5.4).

In figure 5.9 the calculated charge carrier density p_{int} in the PPV at the PPV/PFO interface is plotted as a function of the electric field in the PFO accepting layer. It is found that the

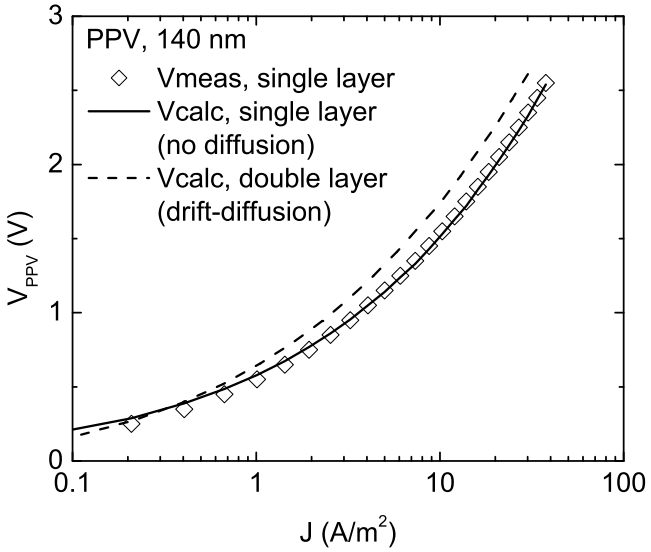

Figure 5.8: Voltage drop across the PPV-layer V_{PPV} ($d_{PPV} = 140$ nm) as a function of device current. The diamonds show the measured voltage drop for the single layer device (ITO/PPV/Au). The solid line is calculated for the single layer, and without taking account of diffusion. The dashed line is calculated for the double layer, with the drift diffusion device model (figure 5.7).

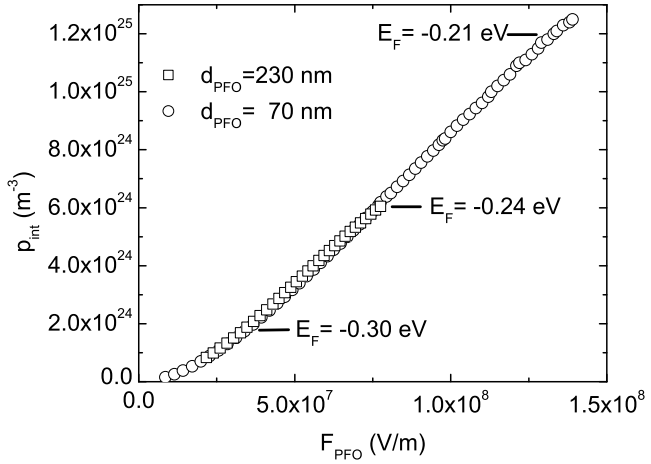

Figure 5.9: Charge carrier density in the PPV at the OOI interface as a function of the electric field in the PFO layer. The squares show the result for a $d_{PFO} = 230$ nm device ($d_{PPV} = 140$ nm), whereas the circles are obtained from a $d_{PFO} = 70$ nm device ($d_{PPV} = 100$ nm). Also shown are the Fermi-levels for different carrier densities, obtained from equation 5.5.

charge concentration ranges from $p_{int} \approx 2 \times 10^{24}$ m$^{-}3$ at $F_{PFO} = 2.5 \times 10^{7}$ V/m up to $p_{int} \approx 1.2 \times 10^{25}$ m^{-3} at $F_{PFO} = 1.5 \times 10^{8}$ V/m, compared with a site density of $N_{sites} = 3 \times 10^{26}$ m^{-3} for PPV-based polymers [42]. Thus, already at low current densities there is a substantial filling of the PPV-DOS near the heterojunction interface. In our measurement range the Fermi-level always lies above the equilibrium energy, σ^2/kT, and therefore determines the effective energy barrier, $\phi_{b,eff} = \phi_b - E_F$.

5.5.3 Modified OOI model

Taking this filling of the PPV-DOS at the heterojunction into account, the injection current has been recalculated with the OOI model. For a given electric field at the heterojunction the corresponding density at the interface is obtained from figure 5.9. Then, from equation 5.5 the position of the Fermi-level in the Gaussian is calculated, from which the effective barrier for injection is obtained. This effective barrier is used in the injection model, represented by equation 5.1, to calculate the modified injection-limited current across the OOI. This procedure has been repeated for a number of fields, as shown in figure 5.10 (crosses). For the width σ of the Gaussian DOS of the PPV a value of 0.11 eV has been used [44].

As shown in figure 5.10 such a correction indeed increases the field-dependence of the current across the organic heterojunction at low fields, but not strong enough to be in agreement with the experimental data. At higher fields the corrected model exhibits a weak field-dependence, similar to the uncorrected model where injection was assumed to start only from the center of the Gaussian DOS. This is because at high fields the Fermi-level approaches the center of the Gaussian and its shift with carrier density will become small due to the large number of available states.

The fact that the corrected model still does not predict the steep field dependence of the experimental current can originate from a number of reasons; First, the shape of the Gaussian at the interface could be different as compared to the bulk value, as suggested by Baldo et al. [86]. Furthermore, the presence of interface traps could also strongly modify the filling effect at the interface. We have demonstrated in chapter 3 that interface traps play an important role in the injection process of charge carriers in an injected-limited polymer LED. Typical interface trap densities of $N_{it} = 2 \times 10^{16}$ m^{-2} were found for PPV. As an example, we have assumed a uniform trap distribution with density $H_t = 5 \times 10^{25}$ m^{-3}eV^{-1} for energies -0.6 eV $\leqslant E \leqslant$ 0.0 eV, as shown in the inset of figure 5.11. It is observed that the originally Gaussian DOS is modified by a long tail of trap states. The filling of the uniform trap distribution is then responsible for the steep field dependence at low electric field, which weakens when the Fermi-level approaches the middle of the Gaussian DOS.

In figure 5.11 the $J - F_{PFO}$ characteristics of the PPV-PFO heterojunction are plotted for $T = 293$ K and $T = 198$ K. Also shown is the calculated injection current using the modified (Gaussian+uniform trap) DOS. It is demonstrated that such a trap distribution account for the observed injection-limited current across the PPV/PFO heterojunction. At higher fields the T-dependence is in agreement with the model, at low fields the model slightly overestimates the observed T-dependence. The main purpose of this exercise is to demonstrate that filling effects at the organic-organic interface can completely dominate the observed current across the heterojunction. Therefore, for a quantitative analysis of the ILC across an organic-organic heterojunction detailed knowledge about the number and energetic position of the localized

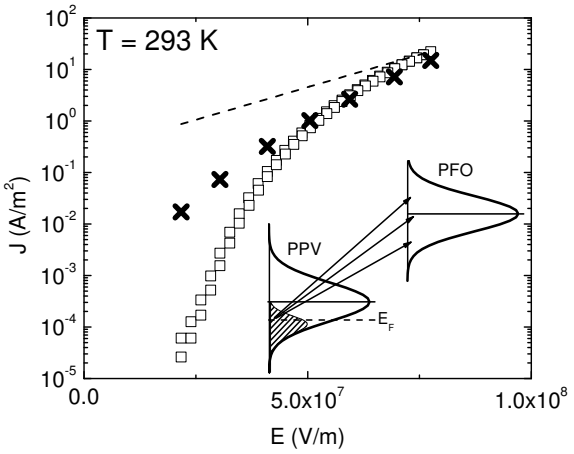

Figure 5.10: The measured current across the PPV/PFO heterojunction ($d_{PPV} = 140$ nm, $d_{PFO} = 230$ nm, squares) together with the calculated injection-limited current over the heterojunction (crosses) for a number of electric fields. This calculation has been performed taking into account the actual Fermi-level for each electric field (see inset), due to the filling of the DOS in the PPV near the heterojunction interface. The dashed line shows the result from the uncorrected model.

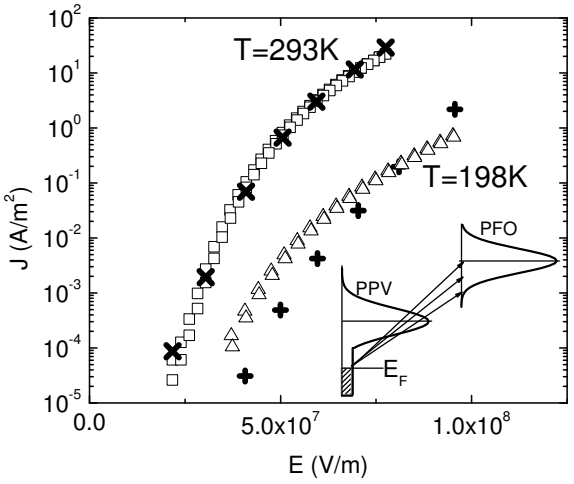

Figure 5.11: Experimental characteristics for $T = 293$ K (squares) and $T = 198$ K (triangles) for a ITO/PPV/PFO/Au device with $d_{PPV} = 140$ nm and $d_{PFO} = 230$ nm, respectively. The crosses (x) and (+) are calculated injection currents from the corrected OOI model, taking into account a Gaussian DOS together with a uniform trap distribution. The inset shows the modified DOS.

interface states is required.

5.6 Application of the heterojunction in a PLED

The advantages of the double layer structure for a PLED have been described in the introduction. To summarize, a heterojunction i)can confine high mobile carriers to a desired area, that has a high emission or is far from a metal interface and ii)can block excitons from diffusing to a metal contact, where they would be efficiently quenched else. In the case of a PPV derivative, like the BEH-BMB-PPV used in this chapter, the holes are the highly mobile carriers and therefore they should be kept away from the metallic cathode. To do so a layer between the PPV and the cathode is required that has a large injection barrier for the holes from the PPV. At the same time, electrons from the cathode must not be blocked by the heterojunction. Furthermore, the excitons generated in the PPV must be prevented from diffusing toward the metal cathode, and therefore the intermediate layer must have a large band gap. As a result, the BEH-BMB-PPV/PFO heterojunction, for which we have investigated the hole injection properties in the first part of this chapter, is an ideal double layer to be used in a PLED, as can be seen from the schematic band diagram of the double layer PLED in the inset of figure 5.12b. The hole injection across this heterojunction is reduced by more than 5 orders of magnitude at low bias (figure 5.3), due to the heterojunction energy barrier for holes. The LUMO of the PPV copolymer and PFO amount to 2.9 eV (Ref. [16]) and 2.6 eV (Refs. [17,18]), respectively. As a result there is no energy barrier for electrons present at the PPV/PFO heterostructure. Furthermore, the bandgap of the PPV copolymer amounts to 2.4 eV, (Ref. [16]) whereas the bandgap of the PFO is about $3.2-3.5$ eV (Refs. [17,18]), resulting in a $0.8-1.1$ eV difference in bandgap. This prohibits transport of excitons through the PFO layer towards the cathode. As a result, it is expected that the reduced conversion effeciency (CE) at low voltages, characteristic of exciton quenching at the cathode [19], is absent in these devices. The double layer has been fabricated on bottom contacts of Indium Tin Oxide (ITO) as well on ITO covered with poly(3,4-ethylenedioxythiophene):poly(styrene sulfonic acid) (PEDOT:PSS). The PPV copolymer bottom layer has a thickness of 180 nm in the single layer device, whereas in the double-layer device a thickness of 160 nm is used. The thickness of the top PFO layer is varied between 20 and 100 nm. As a top contact, barium (Ba) capped with a thick aluminum (Al) layer has been used. Current density - voltage measurements have been taken, and simultaneously the light output is measured with a photodiode. The light intensity L_v is calibrated with a Minolta L110 Luminance meter.

5.6.1 Electro-optical characteristics of double layer PLEDs

In figure 5.12a the current density as a function of voltage is shown for a single layer LED of the PPV copolymer (PPV), as well as double layer LEDs where PFO layers of 20 and 40 nm are added to the PPV layer. The applied voltage is corrected for the built-in voltage V_{bi} of the devices, which typically amounts to $V_{bi} = 1.8$ V. It is observed that the single layer LED and the LED with 20 nm ETL both with a total thickness of 180 nm have similar characteristics, in spite of the presence of the second hole blocking layer. Due the low electron mobility of PFO [83] even an additional layer of only 20 nm is expected to increase the operating voltage of the device. However, the absence of this additional voltage drop in the ETL can be explained

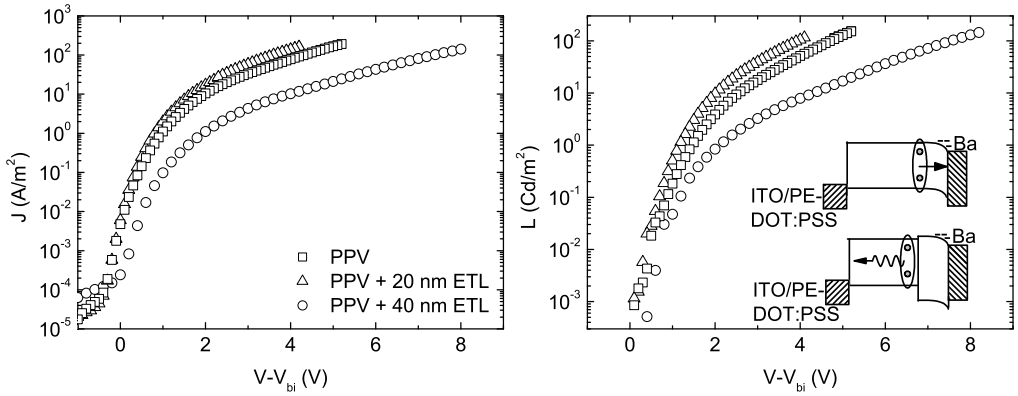

Figure 5.12: Electro-optical characteristics for a single layer PLED and two double layer PLEDs (a) Current density J as a function of internal voltage $V - V_{bi}$ (bias corrected for built-in voltage). The single layer PLED (squares) has a PPV thickness of $d_{PPV} = 180$ nm, whereas the double layer PLEDs have a bottom PPV layer with thickness $d_{PPV} = 160$ nm and different top layer thicknesses $d_{PFO} = 20$ nm (triangles), and $d_{PFO} = 40$ nm (circles). (b) The light output for the same devices. The inset shows a schematic representation of the exciton quenching for a single layer (PPV) and the blocking of the quenching for a PPV/PFO double layer device. Also shown is the band-bending at the cathode due to accumulation. Built-in voltage: $V_{bi} = 1.8$ V.

by accumulation of electrons due to the presence of an Ohmic Ba/Al contact. Calculations with a drift-diffusion device model reveal that this accumulation region (as sketched in the inset of figure 5.12b) typically extends over $\sim$20 nm from the contact in the device. As a result for the device with an ETL of only 20 nm no significant additional voltage drop is present. For the 40 nm ETL device, however, the top layer is thicker than the accumulation length. The resulting extra voltage drop across the ETL consequently shifts the $J - V$ characteristics to higher voltages.

In figure 5.13 the EL spectra of the single layer device (PPV) and the two double layer devices with 20 and 40 nm PFO are depicted, together with the EL of a PFO single layer reference device. It is demonstrated that all the light output of the double layer devices, even down to efficiencies of 0.1%, is emitted by the PPV copolymer layer. This confirms our expectation that the electrons easily travel into the PPV, whereas the holes cannot enter the PFO due to the offset in the HOMO levels. Figure 5.12b shows the light intensity (L_v) of the PPV single layer and PPV/PFO double layer devices (the subscript v denotes the correction for the visual response). Close inspection already indicates that addition of an ETL layer enhances the light output, compared with the current density. In figure 5.14 the conversion efficiency (CE) for the PPV copolymer single layer, as well as the double layer PLEDs with a 20, 40 and 100 nm ETL of PFO are shown. First, it is observed that the single layer PPV based PLED shows the characteristic increase of the CE with applied bias. Model calculations on single layer PLEDs demonstrated that at low voltages most of the excitons are formed close to the cathode, due to the reduced electron transport in PPVs [19]. Since excitons are efficiently quenched by metal

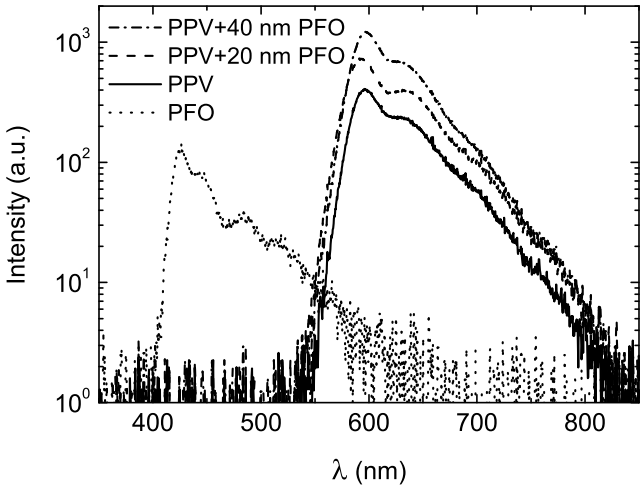

Figure 5.13: Electroluminescence spectra for four PLED devices: the single layer PPV based (solid line), the PPV with a 20 nm PFO top layer (dashed line), the PPV with a 40 nm top layer (dash-dot line), and a bare PFO device (dotted). The EL spectra of all four devices are taken at a current density of typically 100 A/m^2.

contacts [87] such an exciton distribution is expected to result in a low CE at low voltages. For higher voltages the light-generation is more uniformly distributed throughout the PLED device, and exciton quenching becomes less important. As a result, the CE increases gradually with voltage and reaches a maximum at typically 5-8 V.3 Furthermore, these model calculations predicted that the absence of exciton quenching will result in a voltage independent CE, being directly at its maximum value after turn-on.

5.6.2 Reduction of the exciton quenching

From figure 5.14 it appears that for the 20 nm ETL the CE, although already increased at low voltages, still exhibits a gradual increase with voltage, indicative of residual exciton quenching. For the 40 nm and 100 nm ETL, the CE is a block function of voltage, as expected in the absence of exciton quenching [13]. We also observed that the CE for all the devices (no ETL, 20, 40 and 100 nm ETL) tend to collapse on one curve at biases larger than 5 V. Apparently, at sufficiently large bias also in the single layer device exciton quenching becomes insignificant, since excitons are then generated more uniformly throughout the PPV layer. For applications, apart from the CE, the operating voltage of the PLED is also of great importance. This can be expressed in the power efficiency (PE). An increase of the operating voltage will lead to a reduction of the power efficiency, $PE = \frac{L_v}{J \times V}$. In figure 5.15 the power efficiency PE is plotted for the single PPV layer and double layer device with a 20 nm PFO layer. We demonstrate that the addition of an ETL layer of PFO leads to a significant increase of the PE at low voltages. It has already been suggested in literature that the power efficiency will increase for smaller quenching length [88].

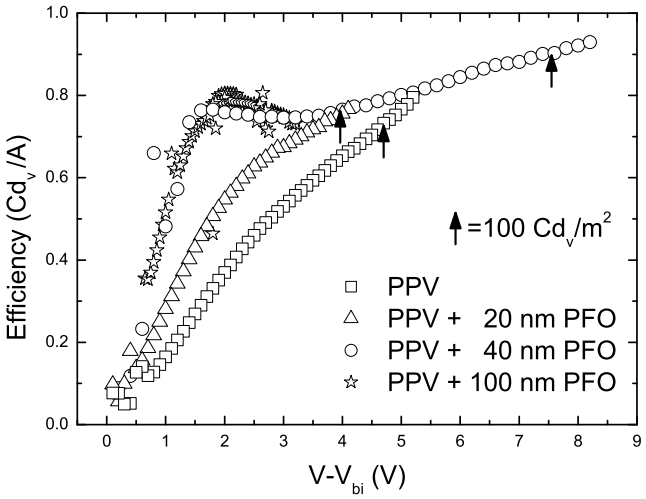

Figure 5.14: Efficiency (Cd_v/A) as a function of internal voltage. The arrows denote the 100 $\mathrm{Cd}_v/\mathrm{m}^2$ point (not shown for the device with 100 nm PFO).

In figure 5.15 it is demonstrated that the addition of a small ETL layer is in accordance with an effective reduction of quenching length. The calculated lines have been performed with a device model [19], for different values of the quenching length in a single layer device. It is demonstrated that the global features of the measured PE are reproduced by the calculation. It is observed from figure 5.15 that the addition of a small ETL layer results in a higher PE at 100 Cd/m^2, as indicated by the arrows. For the same total device thickness, the light output of 100 Cd/m^2 for the double layer device (ETL = 20 nm) is reached at lower voltage and with a better efficiency. Therefore, the PE is improved. It should be noted that addition of a thin ETL layer allows for a thinner luminescent layer, without losing the robustness of the device in terms of shorts. The device with 20 nm ETL has the same total thickness, as a consequence it has a comparable $J - V$ characteristic and due to the reduced exciton quenching it has an enhanced light output. At the other hand, the device with 40 nm ETL, although the exciton quenching is further reduced (figure 5.14), has a lower PE at 100 Cd/m^2, due to the higher operating voltage (7.6 V, figure 5.12b). This reduction of the PE is due to the relatively poor electron transport in PFO [83], as compared to the hole transport in PPV. Therefore, in order to prevent substantial voltage losses, the ETL top layer should not be too thick. The optimum performance therefore is the best compromise between reduction of the exciton quenching and enhancement of the operating voltage, and for PFO as an ETL the optimum is found for an ETL thickness of ~ 20 nm.

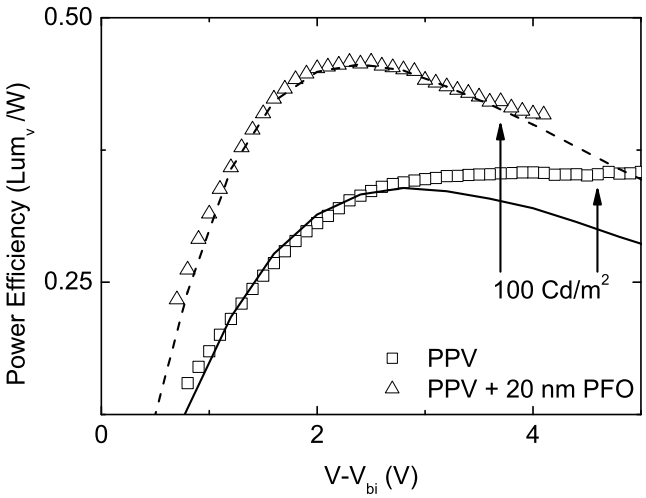

Figure 5.15: Power efficiency (PE) as a function of internal voltage. The symbols show the measured PE for a single layer PPV (squares), and PPV+20 nm PFO (triangles). The lines are calculations of the PE for different quenching lengths: $L_q = 30$ nm (solid), $L_q = 15$ nm (dashed). Again, the arrows indicate the 100 Cd/m^2 point for the measured PE's.

5.7 Conclusions

It has been demonstrated that a polymeric heterojunction strongly limits the hole current due to an interface energy barrier. In order to obtain the intrinsic field dependence of the injection-limited current across the heterojunction the potential drop across the injecting layer, due to the built-up of space charge, has to be taken into account. At high electric fields ($> 10^8$ V/m) the observed weak field dependence, due to the absence of image force lowering, is in agreement with the predictions of the organic-organic interface model by Arkhipov et al. [81]. The strong field dependence at low fields can be explained by a shift of the Fermi-level at the PPV/PFO interface due to an increased charge carrier concentration at higher applied voltage.

Furthermore, we have demonstrated that exciton quenching in PLEDs can be suppressed by deposition of a thin ETL layer on top of the emitting layer. If properly designed this ETL layer prohibits both hole transport and energy transfer towards the metallic cathode. It is demonstrated that a top layer of PFO of 40 nm is sufficient to completely suppress exciton quenching. However, due to the relatively poor electron transport in PFO the power efficiency for a 40 nm ETL is reduced. A 20 nm ETL of PFO is a better compromise for simultaneously improving the conversion- and power efficiency.